Mean stress effect during cyclic stress/straining of 42CrMo4 structural steel

L. Reis, B. Li and M. de Freitas

Department of Mechanical Engineering, Instituto Superior Técnico
Av. Rovisco Pais, 1049-001 Lisboa, Portugal; Fax: +351 218417915
E-mail: luís.g.reis@ist.utl.pt, bli@ist.utl.pt, mfreitas@dem.ist.utl.pt

ABSTRACT. *The mechanism of the mean stress effect during cyclic stress/straining of 42CrMo4 steel was investigated. Since the 42CrMo4 steel is widely used for shafts and other components under complex loading conditions, this paper focus on its mechanical behaviour subject to combined axial/torsion loads. Both experimental and numerical methods are employed in this study. A series of biaxial load controlled fatigue experimental tests were carried out on a biaxial servo-hydraulic testing machine. Experiments were conducted on specimens subjected to cyclic tension/compression with positive and negative mean stress and cyclic tension/compression with a steady torsion, relaxation of the torsion stress was observed. Elastic-plastic finite element analysis was carried out using two different hardening rules: one is the multilinear kinematic hardening model and another one is the Jiang and Sehitoglu´s plasticity model, models give different results in this analysis. Comparisons between the numerical results and experimental results show good agreement.*

INTRODUCTION

Cycle dependent relaxation may alter mean stress (residual stress) values and thus affect fatigue crack initiation life. This phenomenon is an issue both for accuracy of estimated fatigue lives and for the success of methods of intentionally introducing beneficial mean stresses (compressive residual stresses) by several methods such as shot peening, laser peening, low plasticity burnishing, ultrasonic impact treatment and deep rolling, etc. However, residual stress relaxation may occur due to several reasons including thermal, static mechanical load, cyclic load and crack extension effects. Therefore, it is of paramount importance for component design and life management to assess the relaxation of the residual stress (mean stress) field throughout the service life.

Relaxation and redistribution of residual stresses occur when the summation of the residual and applied stresses due to subsequent mechanical loading exceeds the yield condition of the material. In addition, repeated fatigue cycling may induce residual stress relaxation, even when the mechanical load cycles do not cause macroscopic plastic deformation. The extent of cyclic stress relaxation depends on applied loads as well as on the cyclic properties of the materials. This topic has received extensive

attention in the literature, especially for conventional and stainless steels, aluminium alloys as well as titanium alloys [1-3].

Experimental investigations [4-6] indicated, especially at high load levels, significant residual stress relaxation (up to 50%) during the first few loading cycles, followed by a linear logarithmic decrease relationship between residual stresses and load cycles. Besides, a number of combinations of load and material have been investigated and some relaxation models have been proposed in the literature, the elastic–plastic finite element analyses were also used to predict the residual stress relaxation using different material models [7].

A number of different models have been developed for including mean stress effects in fatigue life calculations, such as those of Goodman, of Morrow, and of Smith–Watson–Topper (SWT) [8]. However, much research efforts have been paid to study the uniaxial mean stress relaxation under cyclic axial strain, very little attention has been paid to study the cycle dependent mean stress relaxation under multiaxial loading conditions. For example, the cyclic torsion strains alter the axial mean stress, and so on.

The objective of this paper is to study the mean stress effect and interaction behaviour of 42CrMo4 steel under multiaxial loading conditions. Both experimental and numerical methods are employed in this study. A series of biaxial load controlled fatigue tests were carried out on a biaxial servo-hydraulic testing machine, different loading paths were carried out to study the cycle dependent mean stress relaxation and the fatigue behaviour. Finite element analysis was carried out on same geometry and correspondent loading paths, using the cyclic stress strain curve and kinematic hardening model with von Mises yield criterion and associative flow rule. The results obtained are discussed and allow an understanding on the effects of mean stress and stress relaxation, in multiaxial fatigue conditions.

MATERIAL, SPECIMEN AND EXPERIMENTAL PROCEDURE

A low alloy steel 42CrMo4 heat treated, quenched and tempered (500ºC) was used in this study. Mechanical properties of the studied material are presented in Table 1.

Table 1. Monotonic and uniaxial cyclic mechanical properties of 42CrMo4 steel

Tensile strength	Su (MPa)	1100
Yield strength	Sy (MPa)	980
Young’s modulus	E (GPa)	206
Elongation	A (%)	16
Cyclic Yield strength	Rp0.2, (MPa)	640
Strength coefficient	K´(MPa)	1420
Strain hardening exponent	n´	0.12

Two geometries of specimens were used and are shown in Figs. 1 and 2, respectively. The specimens were machined from 25.0 mm diameter bars. After machining, the specimens were polished. Tests were carried out using a biaxial servo-hydraulic machine (8800 Instron). All the low cyclic fatigue tests were fully reversed on the axial direction (R=-1, strain controlled) with an initial applied torque in rotation angle control (see Fig. 3a), to study the influence of a steady torsion stress in the cyclic stress-strain curve, at a frequency from 0.1 to 1.0 Hz depending of the strain amplitude and performed at room temperature. The load controlled tests were carried out at a frequency of 5 Hz, in cyclic tension-torsion loading paths, with possitive mean stress (see Fig. 3b) and negative mean stress (see Fig. 3c), at room temperature in laboratory air.

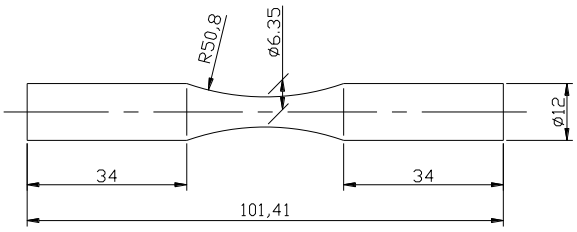

Figure 1. Geometry and dimensions of the specimen 1 (Load controlled tests).

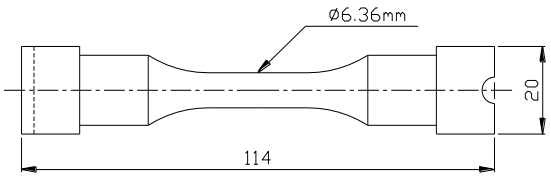

Figure 2. Geometry and dimensions of the specimen 2 (Strain controlled tests).

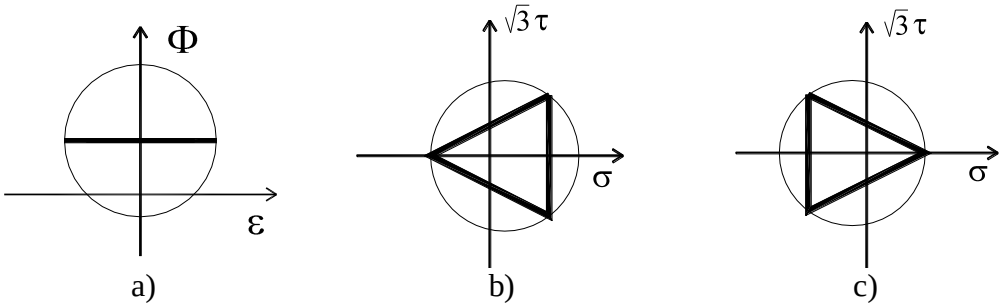

Figure 3. Loading paths carried out in: a) axial strain control – fixed rotation; b) load control - positive mean stress; c) load control - negative mean stress.

NUMERICAL MODELLING

Elastic plastic finite element analyses were carried out using ABAQUS finite element code [9]. The FE mesh and boundary conditions are shown in Fig 4.

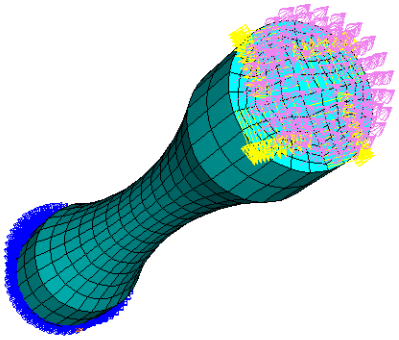

Figure 4. FE mesh used in numerical modelling.

Isoparametric solid elements with 20 nodes were used. For elastic solutions, a course mesh with 784 elements and 3705 nodes were used. For elastic-plastic FEA, the mesh is refined to be with 1372 elements and 6297 nodes. The rate-independent, incremental theory of plasticity has been used for the finite element calculations. In particular, the plasticity theory uses the von Mises yield surface model with associated plastic flow rule. In order to compare the results, two different hardening rules were used: one is the multilinear kinematic hardening model and another one is the Jiang and Sehitoglu´s plasticity model [10].

RESULTS AND DISCUSSION

Experimental Results

For the tests on bi-axial low cycle fatigue (see Fig. 3a), a wide range of axial strains and torque were performed. The objective was to determine the behaviour of the cyclic stress-strain curve on both the elastic and plastic range, i. e. for elastic axial strain and torsional stress, elastic axial strain with plastic torsion, plastic axial strain with elastic torsion stress and both plastic axial strain and torsional stress. Significant results are now presented on Fig. 5. Fig. 5a) shows the plot of the stabilized stress strain curve of three tests respectively with total strain of 0.2% on the elastic region, 0.47% on the transient region and 0.8% on the plastic region, with an initial imposed torque of 16 N.m, which represents a maximum torsional stress just below the elastic limit. Fig. 5b) shows the evolution of an initial torque of 16 N.m applied to specimens with different ranges of strain, during the initial ten cycles. Tests clearly show that three different behaviours were obtained: for elastic axial strain the initial torque remains constant throughout the test, while for axial plastic strain the torque decays significantly on the very first cycles and this torque relaxation is faster for higher axial strains.

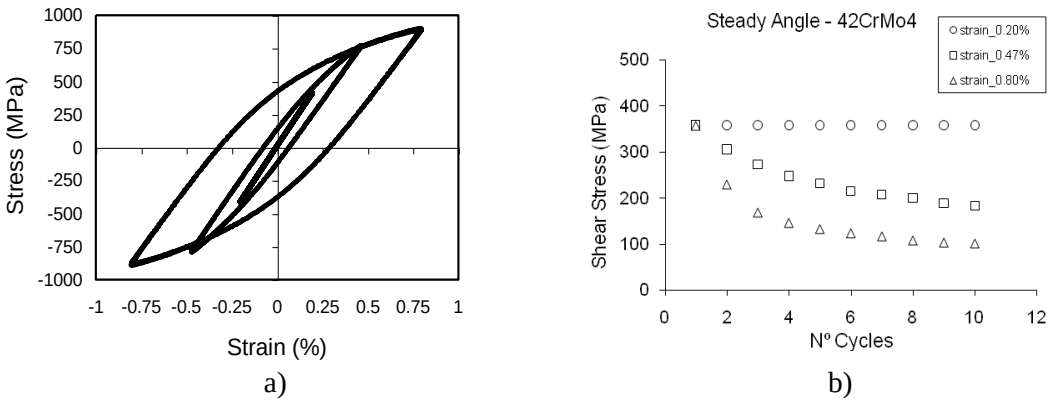

a) b)

Figure 5. Applied torque and steady angle with: a) Stabilized stress strain loops at 0.2%, 0.47% and 0.8%; b) Evolution of torque behavior with cycling.

The effect of two different levels of initial applied torques, respectively 20 N.m and 16 N.m, one giving an initial maximum torsional stress above the yield stress and another below, for the same axial strain of 0.8% (plastic domain) and 0.2% (elastic domain) were also studied.

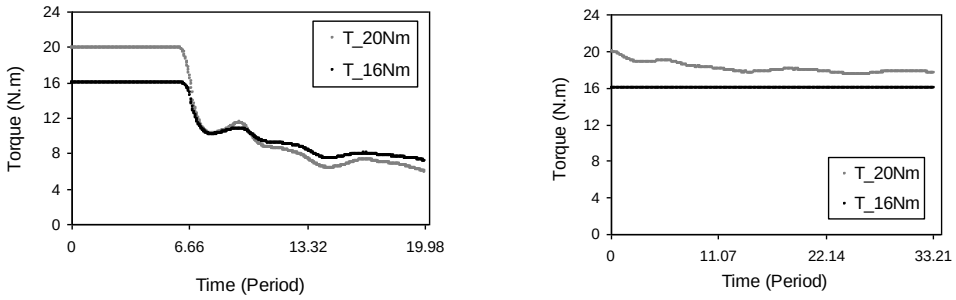

a) b)

Figure 6. Torque relaxation within: a) axial plastic strain - 0.8%; b) axial elastic strain – 0.2%.

Results presented in Fig. 6a), for the case of 0.8% strain, show a stronger decay of the torque for a higher initial torque. In Fig. 6b), the results for initial axial elastic strains, 0.2% strain, show a stress relaxation of the 20 N.m torque only (maximum torsional stress above the yield stress) but the respective torsional stress relaxation remains on the elastic limit.

Experimental tests were also carried out in load control with the loading paths described in Figs 3b) and 3c). Neither shear strain nor axial strain were measured during these tests, only fatigue life was obtained.

Simulation Results

Simulated results by the Kinematic hardening model: Computation was carried out for three cycles of loading with kinematic hardening model using the cyclic stress-strain curve determined in preliminary tests and attention was given to the elements representing the most stressed points, where local approach analysis should be performed. Axial strain versus shear strain curves were plotted on Figs 7 and 8, showing the strain path during the first three cycles of loading.

Fig. 7 shows the evolution of shear strain vs. axial strain due to negative mean stress of the first three cycles for the loading path of Fig. 3c), with an axial stress of ± 500 MPa and a shear stress of ± 220 MPa. After a few cycles the hysteresis loops stabilized to a stable stress-strain loop. Fig. 8 shows the evolution of shear strain vs. axial strain due to positive mean stress of the first three cycles for the loading path of Fig. 3 b), with an axial stress of ± 500 MPa and shear stress ± 220 MPa. After a few cycles the hysteresis loops stabilized to a stable stress-strain loop.

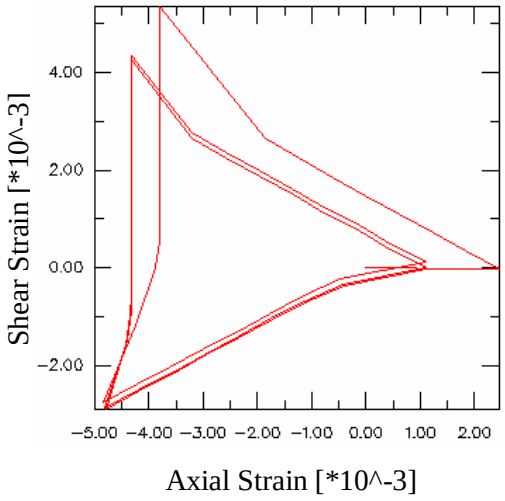

Figure 7. Evolution of shear strain vs. axial strain due to negative mean stress.

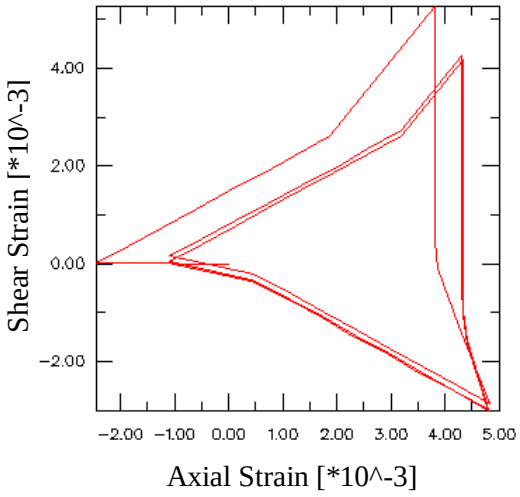

Figure 8. Evolution of shear strain vs. axial strain due to positive mean stress.

Simulated results by the Jiang and Sehitoglu´s plasticity model: One of the recent incremental multiaxial cyclic plasticity models has been proposed by Jiang and Sehitoglu [10]. This model was used in the study of the present paper. The following Fig. 9 shows the loading state of a steady shear strain (fixed angle) with cyclic axial straining, and Fig. 10 shows the simulated torsion stress relaxation due to cyclic axial straining. Good agreement was shown by comparisons of the simulated results shown in Fig. 10 with the test results shown in Figs 5 and 6.

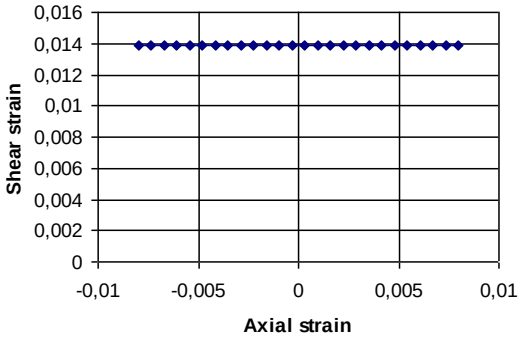

Figure 9. The loading state of steady shear strain with cyclic axial straining.

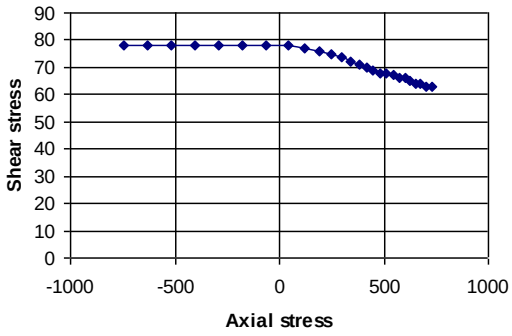

Figure 10. Simulated torsion stress relaxation due to cyclic axial straining.

Figs 11 and 12 show the obtained results of shear strain vs. axial strain computed from load control (applied nominal stresses) for loading cases with negative mean stress and positive mean stress, respectively (see Fig.3b) and c)). Fig. 11 shows the stabilized strain path for the loading path of Fig. 3b) with an axial stress of ± 500 MPa and a shear stress of ± 220 MPa. Fig. 12 shows the stabilized strain path for the loading path of Fig. 3c) with an axial stress of ± 500 MPa and a shear stress of ± 220 MPa.

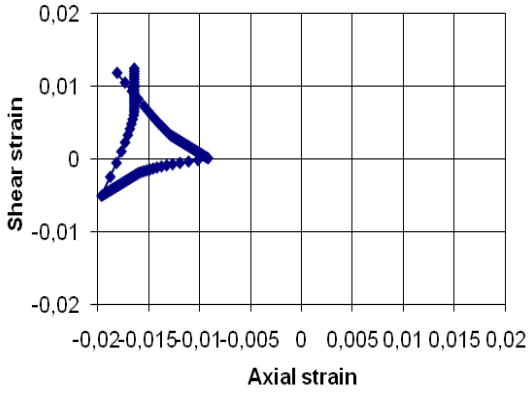

Figure 11. Evolution of shear strain vs. axial strain due to negative mean stress.

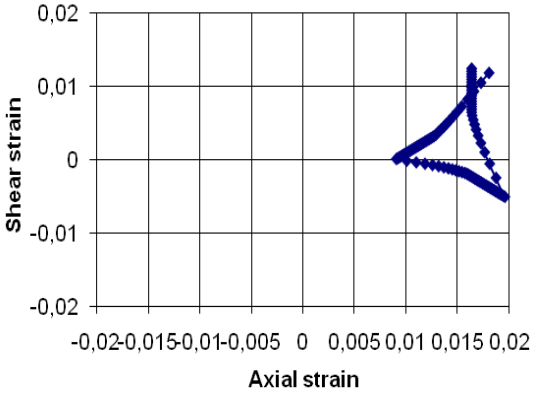

Figure 12. Evolution of shear strain vs. axial strain due to positive mean stress.

Looking to the geometrical aspect of the computed strain path, it seems a triangle, similar to the one present in Figs 7 and 8, but observing the values of the strains the results are quite different from the obtained ones in Figs 7 and 8, namely the axial strains are larger, almost 3 times bigger, and all negative or positive, considering if the applied mean stress is negative or positive, respectively. These results show how important is the plasticity model used, in particular when non proportional multiaxial loading conditions are being carried out.

CONCLUSIONS

In the present study, loading control was applied due to the consideration that plain stress state generally occurs on the surface of components. Therefore, it would be helpful to understanding the stress-strain evolutions under the stress control conditions.
The mechanism of the mean stress effect during cyclic stress/straining of 42CrMo4 steel was studied in this work in both, experimental and numerical methods. The obtained results allow concluding:
- The relaxation of the torsion stress was observed when fully plastic strain was applied. In the case of elastic conditions the torque remained constant.
- Simulations by Jiang and Sehitoglu´s plasticity model give larger values of strains comparing with kinematic hardening model.
- The simulated results agree well with experimental results.

ACKNOWLEDGEMENTS

The work was financed by FCT – Fundação para a Ciência e a Tecnologia, Portuguese Science Foundation through the Project PTDC/EME-PME/104404/2008. The authors are grateful to Prof. D. Socie of UIUC for providing software of implementation of the Jiang and Sehitoglu´s plasticity model.

REFERENCES

1. Benedetti, M., Fontanari, V. and Monelli, B. D. (2010) Transactions of the ASME, *Journal of Engineering Materials and Technology*, **132**, 011012-1 – 9.
2. Arcari, A., De Vita, R. and Dowling, N. E. (2009) *International Journal of Fatigue* **31**, 1742–1750.
3. McClung, R. C. (2007) *Fatigue Fract. Eng. Mater. Struct*., **30**, 173–205.
4. Zinn, W. and Scholtes, B. (1999) *Journal of Materials Engineering and Performance*, **8**, 145–151.
5. Zhuang, W. Z. and Halford, G. R. (2001) *Int. J. Fatigue*, **23**, S31–S37.
6. Beghini, M. and Bertini, L. (1990) *Eng. Fract. Mech.* **36**(3), 379–387.
7. Smith, D.J., Farrahi, G.H., Zhu, W.X. and McMahon, C.A. (2001) *International Journal of Fatigue* **23**, 293–302.
8. Smith, KN, Watson, P and Topper, T.H. (1970) *J Mater ASTM***, 5**(4), 767–778.
9. ABAQUS 6.5-4: Abaqus Theory Manual. Hibbitt, Karlsson & Sorensen, Inc. (2001).
10. Jiang, Y. and Sehitoglu, H. (1996) *Journal of Applied Mechanics*, **63**, 720-725.
11. Stephens, R. I., Fatemi, A., Stephens, R.R. and H. O. Fuchs (2001) Metal Fatigue in Engineering, Wiley Interscience, 2nd edition.